

Cooling history of the Pacific lithosphere

Michael H. Ritzwoller, Nikolai M. Shapiro, & Shi-Jie Zhong

Department of Physics, University of Colorado at Boulder, Boulder, CO 80309-0390 USA

Plate tectonics is expressed most simply in oceanic plates where a thermal boundary layer or “lithosphere” forms as the plate cools during its journey away from mid-ocean ridges¹⁻². Based on a seismic model of the Pacific upper mantle inferred from a new compilation of seismic surface wave dispersion measurements, we show that, on average, the Pacific lithosphere has experienced a punctuated cooling history, cooling diffusively for its first 70 Ma and then reheating in the Central Pacific between ages of 70 and 100 Ma predominantly at depths between 70 and 150 km. From 100 Ma to about 135 Ma, the processes of reheating are substantially weaker than in the Central Pacific, on average, and the lithosphere undergoes a second phase of diffusive cooling. The cause of the reheating in the Central Pacific remains unclear, although thermal plumes at a number of length scales are probably important, particularly to modulate thermal boundary layer instabilities (TBI). We show, however, that TBI forms naturally as the plate cools and, with the right rheology, can explain the average characteristics of the observed cooling history of the Pacific plate.

Few observables directly constrain the thermal state of the oceanic lithosphere or the “asthenosphere” that lies beneath it. Seafloor topography and heat flow³⁻⁵ have been most commonly used to infer oceanic mantle temperatures as these surface observables reflect the average temperature and the temperature gradient in the uppermost mantle. The lithosphere is believed to cool with age because of the deepening of the sea-floor and the reduction in heat flow away from the mid-ocean ridges, but these trends cease and topography becomes much more erratic by about 80 Ma. Seismic waves provide a more direct probe of mantle structures, and seismic models have recently revealed that the Central Pacific hosts several intriguing features, including anomalous asthenospheric radial anisotropy⁶, changes in the strength and orientation of azimuthal anisotropy^{7,8}, and the existence of upper mantle and transition zone anelastic anomalies⁹. The application of seismic models to sub-oceanic lithospheric geothermometry, however, has been limited due to substantial uncertainties in the conversion from seismic velocities to temperatures and by poor station coverage across the Pacific seafloor which has reduced both lateral and, more significantly, vertical resolution. Both issues have been increasingly ameliorated in recent years due to the growth of the global seismic network and advances in the theory of thermoelasticity¹⁰.

Surface waves provide the most uniform coverage of the Pacific lithosphere of all seismic waves and now densely sample most of the Pacific basin (see supplementary information). Observations of surface wave dispersion strongly constrain shear velocities which are related to temperatures in the uppermost mantle¹⁰. Using information about surface wave dispersion across the Pacific we estimated a radially anisotropic (transverse isotropy with a radial symmetry axis) three dimensional (3-D) tomographic model of shear-wave speed in the Earth’s upper mantle by a Monte-Carlo method¹¹ using both seismic and temperature parameterizations. Inferences are similar from both parameterizations (see supplementary information), but we present results only from the temperature parameterization, which is based on a thermal model of the oceanic lithosphere and asthenosphere¹² with two principal mantle unknowns. The first unknown is the “apparent thermal age” of the lithosphere which is the age at which a conductively cooling half-space would match the observed lithospheric temperature structure. The second unknown is the “potential temperature” of the asthenosphere which is the upward continuation to the surface of asthenospheric temperatures following the mantle adiabatic gradient. The results at a point in the Central Pacific are shown in Figure 1.

Figures 2a and 2b present the 3-D shear-velocity model at a depth of 100 km in the uppermost mantle. The general increase in shear-wave speed toward the western Pacific, as seen in Figure 2a, is consistent with the prediction for a diffusively cooling half-space (Half-Space Cooling or HSC model²). In fact, as Figure 2c shows, until about 70 Ma shear velocities at 100 km depth are, on average, in remarkable agreement with the predictions from the HSC model. A systematic deviation from the HSC model appears in the Central Pacific at lithospheric ages that range from about 70 Ma to somewhat more than 100 Ma (Figure 2b, 2c). This deviation appears as a low shear-wave velocity anomaly running largely north-south across the Central Pacific, confined in the era between the 70 Ma and 105 Ma age contours in Figure 2b. The reduction of shear-wave speed in this era is robust to data subsetting, to changes in the theory of wavefield sensitivity (ray versus diffraction tomography), to ad-hoc choices of damping, and is a persistent feature of the inversion. Above and below 100 km depth, the pattern of the deviation is similar but the amplitude decreases (Figure 2d, 2e). As seen in Figure 2f, the average Pacific isotachs deepen with lithospheric age, following the HSC model until about 70 Ma and then flatten until about 105 Ma, after which they deepen again. This deviation is shown in Figure 2g to set-on abruptly at about 70 Ma and maximizes in the deep lithosphere and shallow asthenosphere at depths between 70 km and 150 km. The approximately uniform deviation below 100 km seen in Figure 2g is caused by the fact that the HSC model does not include adiabatic heating with depth.

The same trend with lithospheric age is revealed in the thermal structure seen in Figure 3.

Lithospheric temperatures are summarized by the apparent thermal age, shown in Figure 3b. The apparent thermal age diverges systematically from the lithospheric age at about 70 Ma and remains depressed throughout most of the old Pacific (Fig. 3c). The average Pacific isotherms deepen with lithospheric age, as Figure 3d shows, agreeing with the HSC model until about 70 Ma where they flatten until about 100 Ma and deepen until about 135 Ma. The deficit in apparent lithospheric age that exists in the Central Pacific, referred to elsewhere as thermal resetting or extent of rejuvenation⁵, is seen in Figure 4 to grow until it reaches nearly 40 million years at a lithospheric age of 100 Ma. After this age, the age deficit is approximately constant, on average, but becomes highly variable in the very old Pacific at lithospheric ages greater than about 135 Ma.

Our results demonstrate that the seismic and thermal structures of the Pacific lithosphere deviate systematically from a model whose heat flux is dominated by diffusive cooling alone. Although temperatures of formation may have been higher between 70 Ma and 100 Ma than they were prior or subsequent to this era¹³, the temperature anomalies observed in Figure 3c are probably too large to be the residual of elevated temperatures of formation and we do not find elevated average temperatures during this era in other oceans (see supplementary information). For these reasons, we conclude that the processes that have reheated the lithosphere are likely to be on-going. The age trend of lithospheric structure, therefore, suggests two phases of Pacific lithospheric cooling, from 0 Ma to 70 Ma and again from 100 Ma to \sim 135 Ma, bracketing an era of lithospheric reheating during which an average thermal resetting of about 35 Ma develops. At ages older than 135 Ma, the thermal state of the lithosphere is highly variable and the statistics of inference are less favorable as the area covered by old lithosphere is small.

The reheating of the Pacific upper mantle has been proposed previously based largely on surface observables, such as seafloor topography and heat flow evidence⁵. Various convective processes have been hypothesized as the cause of lithospheric reheating, including those confined to the upper mantle (e.g., small-scale convection directly beneath the lithosphere^{14–16} or larger scale convection across the entire upper mantle¹⁷) and those that extend considerably deeper into the lower mantle (e.g. hot spot plumes^{18,19} or larger scale limbs of global convection possibly associated with superswells²⁰). Near surface structures, such as the accumulation of sediments, the formation of volcanic edifices, and associated crustal thickening, however, obscure the interpretation of surface observables alone, and our results provide the first direct evidence of the time-history (70 - 100 Ma) and depth extent (70 - 150 km) of reheating.

Recent seismic evidence points to a superplume that may heat the Central Pacific^{6,9}, but the mechanics of heat transport from the upper mantle into the high viscosity lithosphere remain unclear. One possible mechanism is the development of thermal boundary layer instabilities (TBI), or

small-scale convection, that remove the deep lithosphere and replace it with relatively hot asthenospheric material. The development of TBI may, indeed, be triggered and modulated by upwelling thermal plumes²¹, but TBI also develops spontaneously without the influence of plumes as the lithosphere cools and thickens with age^{14–16}. Although the potential role of a thermal plume in the dynamics of TBI has been studied for the Hawaiian swell²¹, superplumes at the Pacific plate scale are not well understood dynamically. For this reason, in order to examine the effects of TBI on lithospheric thermal structure we have simulated TBI without imposing thermal plumes. Convection cells formed as a result of TBI are too small to be imaged directly by our seismic model. Aspects of the larger-scale thermal anomalies apparent in the seismic model, however, may be caused by TBI. We address whether the consequences of TBI can match the average punctuated cooling history of the Pacific lithosphere, in particular lithospheric reheating that occurs in a discrete time interval from 70 to 100 Ma.

Using a 3-D mantle convection model with temperature-dependent viscosity, the simulated TBI initiates when the lithosphere is ~ 70 Ma old, forms convective rolls oriented approximately along to the direction of plate motion with characteristic diameters between 100 - 200 km²⁴, reheats the lithosphere to temperatures higher than in the HSC model^{16,23}, and cools the asthenosphere. The onset time of TBI is controlled mainly by asthenospheric viscosity and activation energy^{16,22,23}, but the temperature anomalies caused by TBI, which determine the extent of lithospheric reheating and its time evolution, depend dominantly on rheological activation energy^{16,23}. Analogous to the seismic results, we quantify the extent of lithospheric reheating by estimating the apparent thermal age of lithosphere by fitting an error function (eqn. 1) to the simulated temperature structure. We find that, with a judicious choice of rheology, TBI can reheat the lithosphere to match the average cooling history of the Pacific lithosphere (Fig. 4 and supplementary information). As shown in Figure 4, after the onset of TBI, the apparent thermal age remains approximately constant for a period of ~ 25 Ma after which the apparent thermal age increases again. Although TBI remains active after 100 Ma, it is less vigorous because of increases in asthenospheric viscosity caused by TBI at younger ages having lowered asthenospheric temperatures²⁴. A good match between the simulated and observed cooling histories results with an effective rheological activation energy of 120 kJ/mol, similar to the value inferred from flexural deformation near seamounts²⁵. Although TBI can explain the average cooling history of the Pacific lithosphere, our simulations do not explain the variation within lithospheric age ranges observed seismically. To explain this variability may require additional physical processes not included in the simulations presented here, such as variations in the conditions of formation of the lithosphere or the effects of thermal plumes.

Methods

Construction of the 3-D shear velocity and temperature models

The inversion for a radially anisotropic 3-D tomographic model of shear-wave velocity and temperature is performed in two steps. In the first step, we compiled a large new data set of broad-band group velocity measurements and produced Rayleigh and Love wave group velocity maps²⁸ on a $2^\circ \times 2^\circ$ grid across the Pacific from 18 sec period to 200 sec for Rayleigh waves and from 20 sec to 150 sec for Love waves. There are more than 200,000 measurement paths world-wide. We also constructed phase velocity maps using measurements compiled at Harvard⁶ and Utrecht²⁹ Universities from 40 sec to 150 sec period. The great length of most wavepaths across the Pacific necessitates considering the path-length dependent spatial sensitivity of the surface waves in order to model wave-front healing and associated diffraction effects²⁸. The joint inversion of group and phase velocities gives better vertical resolution than either data type alone (see supplementary information), providing unique information about the vertical variability of shear velocities in the uppermost mantle.

In the second step, values from the dispersion maps are used to construct a 3-D model on a $2^\circ \times 2^\circ$ grid to 400 km depth based on two separate parameterizations: a seismic parameterization¹¹ and a temperature parameterization derived from a thermal model¹². The seismic parameterization consists of 13 unknowns, seven in the crust and six in the mantle. The crust consists of three layers in which compressional (V_p) and shear (V_s) velocity are free variables as is crustal thickness; all seven crustal unknowns are perturbed from reference values taken from the model CRUST2.0 (G. Laske, personal communication, 2002). Isotropic mantle structure is parameterized with four radial cubic B-splines. The remaining two unknowns parameterize radial anisotropy. Because Rayleigh waves are predominantly sensitive to V_{sv} and Love waves to V_{sh} , we have constraints on only two of the five elastic moduli that describe a transversely isotropic medium. The basis functions for radial anisotropy represent the bifurcation of V_{sh} and V_{sv} in the uppermost mantle to a depth of 220 km and are sufficiently flexible to accommodate the unusual anisotropy in the Central Pacific⁶. The effective isotropic shear velocity, V_s , is defined as the average of the anisotropic velocities.

The inversion proceeds by a Monte-Carlo sampling that walks randomly through a subspace of model space defined by a-priori constraints and forms a Markov-chain similar to Brownian motion. At each point on the $2^\circ \times 2^\circ$ grid, an ensemble of acceptable vertical profiles emerges (e.g., Fig. 1c). The motivation of the Monte-Carlo inversion is to estimate a range of seismic and temperature models at each depth so that only features that appear in every member of the ensemble of acceptable models are interpreted. We refer to these features as “persistent”. When a single model is needed, we use the middle of the ensemble of acceptable models.

The temperature parameterization (Fig. 1a) is based on a thermal model in which a thermally conductive layer (lithosphere) overlies a convective layer (asthenosphere) joined smoothly by a transition layer. The temperature profile within the conductive layer is described by the half-space cooling solution,

$$T(z) = T_s + (T_m - T_s) \operatorname{erf}(z/2\sqrt{\kappa\tau}), \quad (1)$$

where z is depth in the mantle, T_m is initial mantle temperature fixed at 1300°C, $T_s = 0^\circ\text{C}$ is the surface temperature, thermal diffusivity $\kappa = 1 \times 10^{-6} \text{ m}^2\text{s}^{-1}$, and τ is the “apparent thermal age” of the lithosphere. In the convective layer, the adiabatic temperature gradient $D_a = 0.5^\circ\text{C}/\text{km}$ and the potential temperature T_p describe the thermal state of the asthenosphere.

Two mantle unknowns in the temperature parameterization specify the thermal state of the oceanic upper mantle: τ in the lithosphere and T_p in the underlying asthenosphere. These two unknowns replace the four B -splines in the seismic parameterization. The Monte-Carlo inversion with the temperature parameterization initiates in temperature space where a trial thermal model is constructed and converted to shear velocity in the mantle, then trial seismic crustal structures are introduced as well as mantle radial anisotropy similar to the generation of these features in the seismic parameterization. The temperature profiles that fit the seismic data acceptably for an appropriate subset of seismic crustal models and models of radial anisotropy define the ensemble of acceptable profiles in temperature space and are also combined with the crustal and radial anisotropic models to define the ensemble of acceptable models in seismic velocity space.

Interconversion between temperature and shear velocity

Interconversion between temperature and shear velocity is based on laboratory-measured thermoelastic properties of mantle minerals represented as partial derivatives of the elastic moduli with respect to temperature, pressure, and composition¹⁰. The compositional model for the oceanic upper mantle includes 75% Olivine, 21% Orthopyroxene, 3.5% Clinopyroxene, and 0.5% Spinel with an Iron-to-Magnesium ratio of 10%³⁰. We compute shear velocity with the anelastic correction¹⁰ from an anharmonic shear velocity, $v_{anel}(P, T, \omega) = v(P, T) \left[1 - \left(2Q_\mu^{-1}(P, T, \omega) / \tan(\pi a/2) \right) \right]$, using a temperature dependent Q -model, $Q_\mu(P, T, \omega) = A\omega^a \exp[a(H^* + PV^*)/RT]$, where R is the gas constant and we set the exponent $a = 0.15$, anelastic activation energy $H^* = 500 \text{ kJ/mol}$, anelastic activation volume $V^* = 2.0 \times 10^{-5} \text{ m}^3/\text{mol}$, and the amplitude $A = 0.049$.

Half-Space Cooling (HSC) Model

The vertical temperature profile of the HSC model² is the solution to the one dimensional thermal diffusion equation for an infinite half-space, which takes the same form as equation (1). In contrast

with the temperature parameterization for the seismic inversion, the error-function temperature profile for the HSC model continues infinitely with depth and explicitly does not include adiabatic heating. Predictions from the HSC model are intended to represent age trends expected for purely diffusive cooling. Several ad-hoc choices (e.g., T_m , the Q -model) in specifying the HSC model create uncertainty in the absolute level of temperatures and seismic velocities in the mantle. We account for this in Figures 2a-2c, but not elsewhere, by shifting the HSC predictions vertically to fit the observations optimally between 10 Ma and 60 Ma. This shift also approximately corrects for the effect of adiabatic heating.

Simulating Thermal Boundary Layer Instabilities

Our 3-D Cartesian convection model uses a depth- and temperature-dependent Arrhenius rheology with flow-through boundary conditions²⁴. The model box is 1000 km deep, 12,000 km long (in the direction of plate motion), and 3,000 km wide. At the surface, temperature is 0°C and plate velocity is 5 cm/year, while at the bottom of the box temperature is 1350°C and velocity is zero. The inflow boundary has temperatures corresponding to 10 Ma old lithosphere with velocities derived from a Couette flow. The outflow boundary has zero vertical temperature gradient and the same velocities as the inflow. The other two sidewalls (i.e., parallel to plate motion) have reflecting boundary conditions. The viscosity law is $\eta(z, T) = \eta_0(z) \exp(E/RT)$ where the pre-factor $\eta_0(z)$ is constant above 400 km depth and increases by a factor of 19 and 190 in the transition zone and lower mantle, respectively, compared with that in the upper mantle²³. The viscosity in the upper mantle is about 4×10^{19} Pa-s and rheological activation energy is 120 KJ/mol. This leads to ~ 70 Ma onset time for TBI²³. This activation energy is consistent with that inferred from the study of flexural deformation near seamounts²⁵. Because we employ a Newtonian rheology, however, the activation energy may be viewed only as an “effective” rheological parameter for the mantle with a non-Newtonian rheology²⁶. The models are computed to a statistical steady-state. Other model parameters are thermal diffusivity of 10^{-6} m²/s, coefficient of thermal expansion of 3×10^{-5} K⁻¹, mantle density of 3,300 kg/m³, and gravitational acceleration equal to 9.8 m/s².

References

1. McKenzie, D.P., Some remarks on heat flow and gravity anomalies, *J. Geophys. Res.*, *72*, 6261-6273, 1967.
2. Parker, R.L. & Oldenburg, D.W., Thermal model of ocean ridges, *Nature Phys. Sci.*, *242*, 137-139, 1973.
3. Parsons, B. & Sclater, J.G., An analysis of the variation of ocean floor bathymetry and heat flow with age, *J. Geophys. Res.*, *82*, 803-827, 1977.
4. Stein, C. A. & Stein, S., A model for the global variation in oceanic depth and heat flow with lithospheric age, *Nature*, *359*, 123-129, 1992.
5. Nagihara, S., Lister, C.R.B., & J.G. Sclater, Reheating of old oceanic lithosphere: Deductions from observations, *Earth Planet. Sci. Letts.*, *139*, 91-104, 1996.
6. Ekström, G. & Dziewonski, A.M., The unique anisotropy of the Pacific upper mantle, *Nature*, *394*, 168-172, 1998.
7. Ekström, G., Mapping the lithosphere and asthenosphere with surface waves: Lateral structure and anisotropy, in *The History and Dynamics of Global Plate Motions*, ed. M.A. Richards, R.G. Gordon, R.D. van der Hilst, Amer. Geophys. Un. Geophys. Monogr. 121, 239-256, Washington, D.C., 2000.
8. Trampert, J. & Woodhouse, J.H., Global anisotropic phase velocity maps for fundamental mode surface waves between 40 s and 150 s, *Geophys. J. Int.*, *154*, 154-165, 2003.
9. Romanowicz, B. & Gung, Y., Superplumes from the core-mantle boundary to the lithosphere: Implications for heat flux, *Science*, *296*, 513-516, 2002.
10. Goes, S., Govers, R., & Vacher, R., Shallow mantle temperatures under Europe from P and S wave tomography, *J. Geophys. Res.*, *105*, 11,153-11,169, 2000.
11. Shapiro, N.M. & Ritzwoller, M.H., Monte-Carlo inversion for a global shear velocity model of the crust and upper mantle, *Geophys. J. Int.*, *51*, 88-105, 2002.
12. Shapiro, N.M. & Ritzwoller, M.H., Thermodynamic constraints on seismic inversions, *Geophys. J. Int.*, submitted, 2003.
13. Larson, R.L., Latest pulse of Earth: Evidence for a mid-Cretaceous superplume, *Geology*, *19*, 547-550, 1991.
14. Richter, F. M. & Parsons, B., On the interaction of two scales of convection in the mantle, *J. Geophys. Res.*, *80*, 2529-2541, 1975.
15. Parsons, B. & McKenzie, D., Mantle convection and thermal structure of the plates, *J. Geophys. Res.*, *83*, 4485-4496, 1978.
16. Davaille, A. & Jaupart, C., Onset of thermal convection in fluids with temperature-dependent viscosity: application to the oceanic lithosphere, *J. Geophys. Res.*, *99*, 19,853-19,866, 1994.

17. Houseman, G. & McKenzie, D.P., Numerical experiments on the onset of convective instability in the Earth's mantle, *Geophys. J. R. Astron. Soc.*, *68*, 133-164, 1982.
18. Crough, S.T., Thermal origin of mid-plate hot-spot swells, *Geophys. J. R. Astron. Soc.*, *55*, 451-470, 1978.
19. Schroeder, W., The empirical age-depth relation and depth anomalies in the Pacific Ocean, *J. Geophys. Res.*, *89*, 9873-9884, 1984.
20. McNutt, M.K., Superswells, *Revs. Geophys.*, *36*, 211-244, 1998.
21. Moore, W.B., Schubert, G. & Tackley, P., Three-dimensional simulations of plume-lithosphere interaction at Hawaiian Swell, *Science*, *279*, 1008-1011, 1998.
22. Korenaga, J. & Jordan, T. H., Physics of multiscale convection in Earth's mantle: Onset of sublithospheric convection, *J. Geophys. Res.*, *108(B7)*, 2333, 2003.
23. Huang, J., Zhong, S. & van Hunen, J. Controls on sub-lithospheric small-scale convection, *J. Geophys. Res.*, in press, 2003.
24. van Hunen, J., Huang, J., & Zhong, S., The effect of shearing on onset and vigor of small-scale convection with a Newtonian rheology, submitted to *Geophys. Res. Lett.*, 2003.
25. Watts, A.B. & Zhong, S., Observations of flexure and the rheology of oceanic lithosphere, *Geophys. J. Int.*, *142*, 855-875, 2000.
26. Christensen, U. R., Convection with pressure and temperature dependent non-Newtonian rheology, *Geophys. J. R. Astron. Soc.*, *77*, 242-284, 1984.
27. Mueller, R.D., Roest, W.R., Royer, J.-Y., Gahagan, L.M., & Sclater, J.G., Digital isochrons of the world's ocean floor, *J. Geophys. Res.*, *102*, 3211-3214, 1997.
28. Ritzwoller, M.H., Shapiro, N.M., Barmin, M.P., & Levshin, A.L., Global surface wave diffraction tomography, *J. Geophys. Res.*, *107(B12)*, 233, 2003.
29. Trampert, J. & Woodhouse, J.H., Global phase velocity maps of Love and Rayleigh waves between 40 and 150 s period, *Geophys. J. Int.*, *122*, 675-690, 1995.
30. McDonough, W.F. & Rudnick, R.L., Mineralogy and composition of the upper mantle, in: *Ultrahigh-pressure mineralogy: physics and chemistry of the Earth's deep interior*, R.J. Hemley, Editor, 139-164, Mineralogical Society of America, Washington, DC, 1998.

Acknowledgments. The data used in this work were obtained from the IRIS Data Management Center and the GEOSCOPE Data Center. The authors are grateful to researchers at Harvard and Utrecht Universities for contributing phase velocity measurements to this study. We thank Anatoli Levshin, William Landuyt, Rosa Bernal, Liz Zea, and Abir van Hunen for help in preparing the data set. Aspects of this work were supported by the US National Science Foundation and the Packard Foundation.

Supplementary information accompanies the paper at:

http://ciei.colorado.edu/pubs/2003/7_suppl.pdf

Competing interests statement. The authors declare that they have no competing financial interests.

Correspondence and requests for materials should be addressed to M.H.R. (ritzwoller@ciei.colorado.edu)

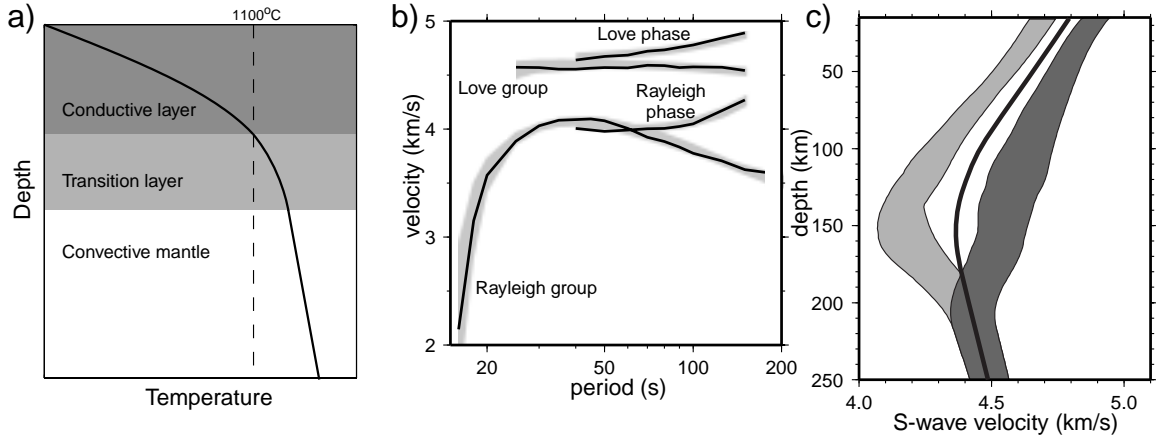


Figure 1: **Thermal parameterization and inversion at a point in the Central Pacific.** (a) The thermal parameterization is defined by an error function that represents temperatures in the lithosphere (eqn. 1) underlain by an adiabatic gradient in the convective mantle (asthenosphere), joined smoothly by a transition region. (b) & (c) Inversion results for a point in the Central Pacific (14°N, 200°E). Predictions from the ensemble of acceptable models (grey lines) to the four observed dispersion curves (black lines) are shown in (b). The ensemble of acceptable models in the uppermost mantle is shown in (c), where the light grey-shaded envelope is V_{sv} and the dark grey-shaded envelope is V_{sh} . The solid line is the median of the ensemble of isotropic shear velocities, V_s , which derives directly from the thermal model. This example demonstrates the unusual anisotropy in the Central Pacific⁶ in which the bifurcation between V_{sv} and V_{sh} grows with depth, maximizing at about 150 km.

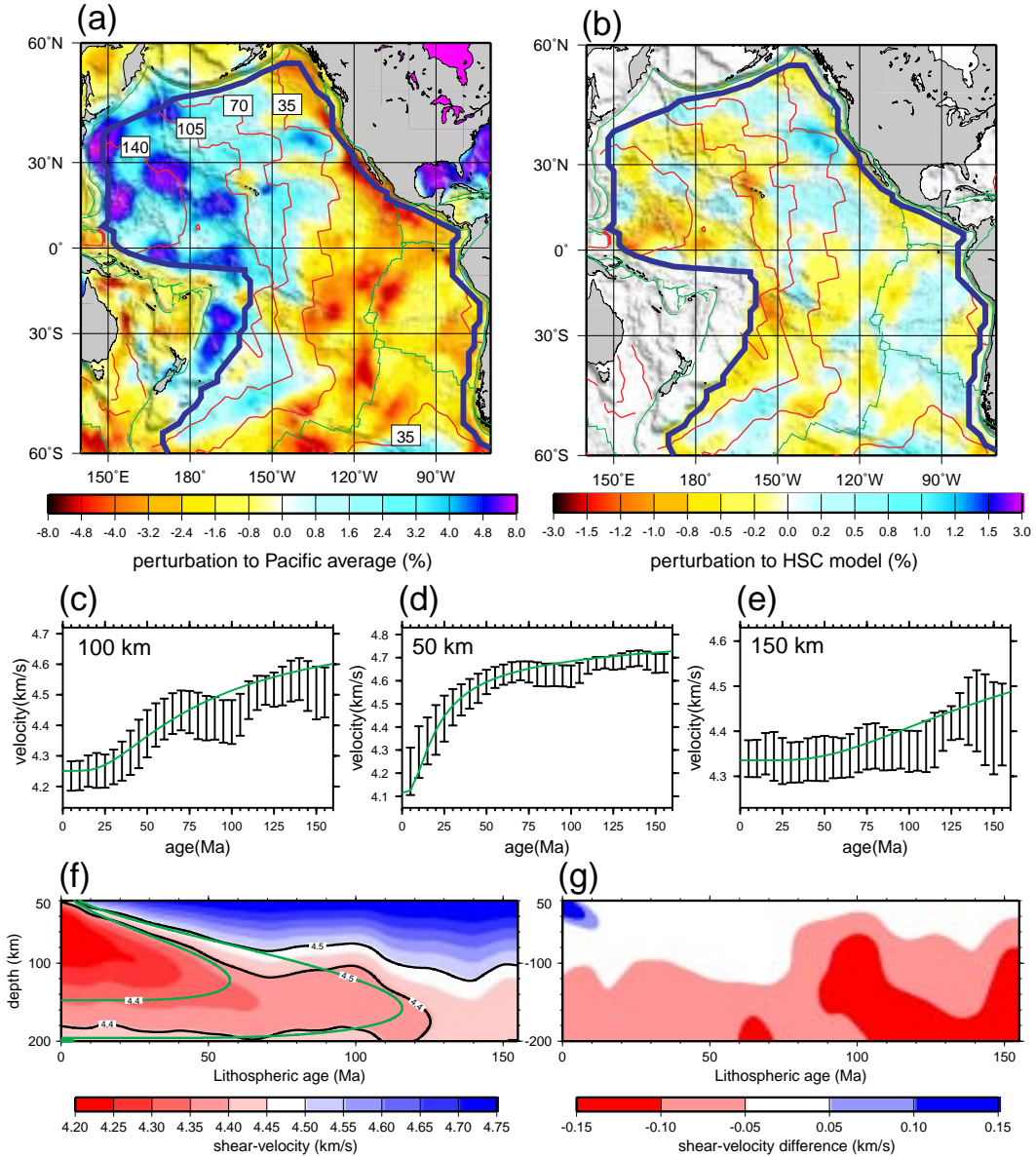


Figure 2: Shear velocity structure of the Pacific upper mantle and trend with lithospheric age. (a) Isotropic shear velocity, V_s , at 100 km depth, as a perturbation to the average across the Pacific (4.362 km/sec). The green lines denote plate boundaries, the red lines are isochrons of lithospheric age in Ma, and the blue contour encloses the region where there are lithospheric age estimates²⁷. (b) V_s at 100 km depth presented as a perturbation to the prediction from the HSC model. (c) - (e) Shear velocity, averaged in 5 Ma lithospheric age bins across the Pacific, is plotted versus lithospheric age at 100 km, 50 km, and 150 km depth. Error bars represent the standard deviation within each age range. The continuous green lines are the predictions from the HSC model shifted vertically to fit the observations optimally between 10 Ma and 60 Ma: -30 m/s at 100km, -10 m/s at 50 km, and -70 m/s at 150 km. (f) V_s averaged across the Pacific plotted versus lithospheric age. The green lines are isotachs (lines of constant shear velocity) from the HSC model. (g) Difference between the Pacific average V_s and the prediction from the HSC model. Reds identify areas where the observed V_s is slower than the HSC model predicts.

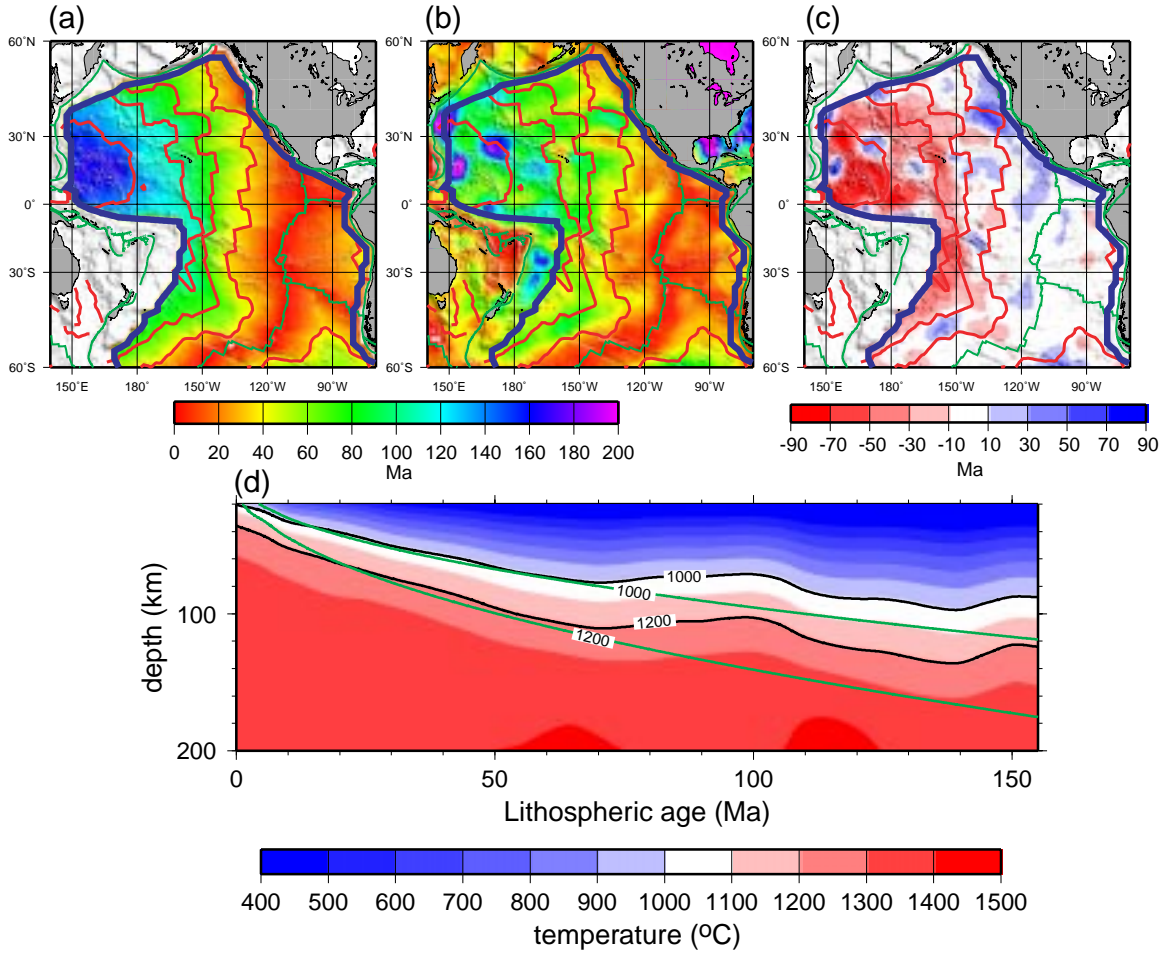


Figure 3: **Thermal structure of the Pacific upper mantle and trend with lithospheric age.** (a) Lithospheric age in Ma, presented as a reference²⁷. (b) Estimated apparent thermal age, τ . (c) Difference between the lithospheric age and the apparent thermal age. Reds denote that the apparent thermal age is younger than the lithospheric age. In (a) - (c), the green, red, and blue lines are as in Figure 2a,b. (d) Upper mantle temperature averaged across the Pacific plotted versus lithospheric age. The green lines are isotherms from the HSC model.

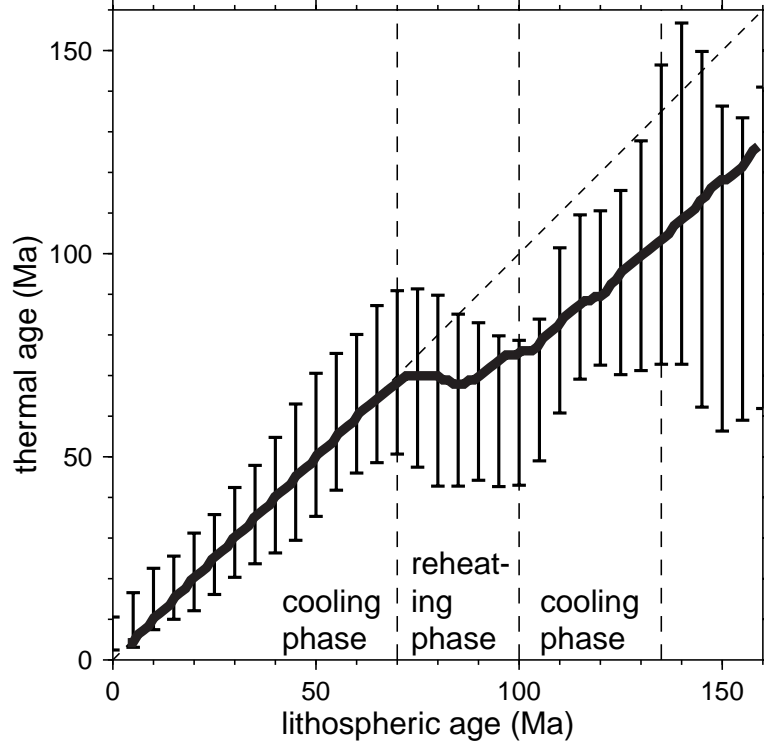


Figure 4: **Comparison between apparent thermal age, τ , with lithospheric age.** The error bars represent the standard deviation of observed τ within each 5 Ma lithospheric age bin averaged across the Pacific. Two lithospheric cooling phases are identified, 0 - 70 Ma and 100 - 135 Ma, bracketing a phase in which the Pacific lithosphere undergoes reheating. The thick black line is τ , similarly averaged in lithospheric age bins, computed from the 3-D convection model of thermal boundary layer instabilities, with an effective rheological activation energy of 120 kJ/mol.